Eur. Phys. J. B **58**, 127–133 (2007)
DOI: 10.1140/epjb/e2007-00209-1

THE EUROPEAN PHYSICAL JOURNAL B

Ab-initio simulation of elastic constants for some ceramic materials

M. Iuga[1,a], G. Steinle-Neumann[2,b], and J. Meinhardt[1]

[1] Fraunhofer Institut – Silicatforschung (ISC), 97082 Wuerzburg, Germany
[2] Bayerisches Geoinstitut, University of Bayreuth, 95440 Bayreuth, Germany

Received 21 December 2006 / Received in final form 15 June 2007
Published online 1st August 2007 –

Abstract. Athermal elasticity for some ceramic materials (α-Al_2O_3, SiC (α and β phases), TiO_2(rutile and anatase), hexagonal AlN and TiB_2, cubic BN and CaF_2, and monoclinic ZrO_2) have been investigated via density functional theory. Energy-volume equation-of-state computations to obtain the zero pressure equilibrium volume and bulk modulus as well as computations of the full elastic constant tensor of these ceramics at the experimental zero pressure volume have been performed. The present results for the single crystal elasticity are in good agreement with experiments both for the aggregate properties (bulk and shear modulus) and the elastic anisotropy. In contrast, a considerable discrepancy for the zero pressure bulk modulus of some ceramics evaluated from the energy-volume fit to the computational zero pressure volume has been observed.

PACS. 31.15.Ar Ab-initio calculations – 71.15.Mb Density functional theory, local density approximation, gradient and other corrections – 62.20.Dc Elasticity, elastic constants

1 Introduction

Over the last decades ceramics have become key materials in the development of many new technologies. As scientists and engineers have been able to design these materials with new structures and properties, an understanding of the factors that influence their mechanical behaviour and reliability is essential. Elastic properties of ceramics are important because they govern the reversible response of the crystal to external forces, determining their performance in numerous applications: refractories are used in iron and steel; abrasives are used for grinding, cutting or polishing; electrical ceramics are used as capacitors, insulators, substrates and integrated circuit packages; chemical and environmental ceramics as filters, membranes, catalysts, and catalyst supports. Another attractive application of ceramics stems from their low density and large elastic moduli; this makes them attractive for improving stiffness, while reducing the weight of machines. Bulk, shear and Young's moduli as well as Poisson's ratio play an important role in strength determination of materials. In addition, knowing the values of elastic constants, valuable information about the bonding characteristic between atoms and structural stability is provided.

Many experimental techniques are available to measure the elastic moduli. Most directly measurement of strain as a function of stress yields the elastic modulus. This technique can be performed accurately at room temperature using strain gauges, but is limited in temperature, as the strain gauges must be reliably attached [1]. In ultrasonic measurements acoustic waves (typically with MHz frequencies) are sent through a single crystal of material and the angular dependence of the propagation velocities can be converted to elastic constants [2]. In Brillouin spectroscopy incident light is scattered by a (transparent) crystal: part of it elastically, from which the velocity of an acoustic wave can be calculated directly [3]. The latter two techniques can be applied in a wide variety of physical environments, e.g. high temperature and pressure. In the past two decades experimental efforts have been supplemented by computational studies on the elastic properties of crystals by ab-initio calculation, based on density functional theory (DFT).

In the present study the ab-initio calculations on the elasticity and equation of state for a wide array of technologically important ceramics — Al_2O_3, SiC, TiO_2, AlN, BN, TiB_2, CaF_2 and ZrO_2 — have been performed. Results obtained were compared with experimental measurements and previous computations. In the following the materials studied are briefly discussed, including key references. Section 2 contains details about the method used

[a] e-mail: iuga@isc.fraunhofer.de
[b] e-mail: g.steinle-neumann@uni-bayreuth.de

Table 1. Crystal structures of the materials studied here. Space group and lattice parameters are given in the first line for each material; the atomic positions in the following lines.

Material	Space group (number)		a (Å)	b (Å)	c (Å)	α (°)	β (°)	γ (°)
	Atom	Position	x	y	z			
Al_2O_3	R-3cR (167)		5.12846	5.12846	5.12846	55.2884	55.2884	55.2884
	Al	4 c	0.145	0.145	0.145			
	O	6 e	0.947	0.553	0.25			
α-SiC	P63mc (186)		3.087	3.087	10.046	90	90	120
	Si	2 a	0	0	0.188			
	Si	2 b	0.333	−0.333	0.438			
	C	2 a	0	0	0			
	C	2 b	0.333	−0.333	0.25			
β-SiC	F43m (216)		4.384	4.384	4.384	90	90	90
	Si	4 a	0	0	0			
	C	4 c	0.25	0.25	0.25			
TiO_2 rut.	P42/mnm (136)		4.594	4.594	2.959	90	90	90
	Ti	2 a	0	0	0			
	O	2 f	0.3053	0.3053	0			
TiO_2 anat.	I41/amds (141)		3.776	3.776	9.486	90	90	90
	Ti	4 a	0	0	0			
	O	8 e	0	0	0.208			
CaF_2	Fm-3m (225)		3.86264	3.86264	3.86264	90	90	90
	Ca	4 a	0	0	0			
	F	8 c	0.25	0.25	0.25			
AlN	P63m (186)		3.11	3.11	4.98	90	90	120
	Al	2b	−0.3333	−0.6667	0			
	N	2b	−0.3333	−0.6667	0.382			
BN	Fm-3m (225)		3.615	3.615	3.615	90	90	90
	B	4 a	0	0	0			
	N	4 c	0.25	0.25	0.25			
TiB_2	P6/mmm (191)		3.0236	3.0236	3.2204	90	90	120
	Ti	1 a	0	0	0			
	B	2 d	0.333	0.666	0.5			
ZrO_2	P21 /c (14)		5.1454	5.2075	5.3107	90	99.23	90
	Zr	4 e	0.2728	0.0337	0.2088			
	O	4 e	0.0773	0.3133	0.3046			
	O	4 e	0.4619	0.7882	0.4362			

to perform the simulations. Results and their discussion are presented in Section 3. Conclusions are given in Section 4.

Alumina (Al_2O_3) exhibits exceptional hardness and high melting temperatures and has been extensively studied [4–7]. It crystallizes in rhombohedral symmetry (Tab. 1) and has six independent elastic constants. Silicon Carbide (SiC) can exist in a number of different crystalline polytypes, which may be classified in hexagonal (H), cubic (C) and rhombohedral (R) space groups [8]. SiC is of particular interest in composite materials where thermal stresses, and hence elasticity, play an important role in the mechanical stability. Two crystal structures of SiC, hexagonal (a) and cubic (ß, zinc-blende type) (Tab. 1), are considered, resulting in five and three independent elastic constants, respectively. Titanium dioxide (TiO_2) is used in a wide variety of applications in the electronics, catalysis, pigment, electrochemical and ceramic industry [9]. TiO_2 forms three distinct polymorphs: rutile, anatase and brookite. The electronic and structural properties of TiO_2 has been widely studied [10–14]. Here the six independent elastic constants of rutile and anatase (both tetragonal, Tab. 1) are computed. CaF_2 is an important ceramic due to its optical behavior and large ionic conductivity, with its elastic behavior studied for decades [15–18]. The three independent elastic constants of this cubic compound (Tab. 1) are computed here. In the last years the interest in the wide band gap semiconductors such as aluminium nitride (AlN), boron nitride (BN) and related compounds has increased considerably. Cubic BN (Tab. 1) has recently received considerable attention because of its extreme values of hardness, thermal conductivity and elastic constants [19]. AlN possesses a lot of remarkable physical properties, e.g. high thermal conductivity and excellent mechanical strength, which make it an attractive material for electronic packaging applications [20,21]. As cubic materials both have three independent elastic constants. Titanium diboride (TiB_2) exhibits high elastic moduli, high hardness and high electrical conductivity due to its unique electronic structure and bonding nature, making it a material of considerable interest for cutting tools, wear resistant coatings and crucibles [22, 23]. As a hexagonal crystal (Tab. 1) TiB_2 has five independent elastic constants. Zirconium dioxide (ZrO_2) has

Table 2. Computational parameters which were used in the simulations for the equation of state and elastic constants. Given are the k-point sampling for reciprocal space integration, the cutoff energy for the basis set, the type of pseudopotential (PS) (norm-conserving NC and ultrasoft US) used. The compression range (in terms of fraction of the experimental zero pressure volume V_0) for equation-of-state computations is also included.

	Al_2O_3	α-SiC	β-SiC	TiO_2 rut.	TiO_2 anat.	CaF_2	AlN	BN	TiB_2	ZrO_2
k-points	85	28	110	50	84	60	84	120	162	39
$E_{cut\text{-}off}$ [eV]	500	400	400	450	550	500	350	400	400	500
PS	US	US	US	US	US	US	US	US	US	US
V range	76.4–	69.3–	64.9–	54.9–	113.6–	36.6–	33.3–	37.3–	20.3–	126.4–
$[A^3]$	90	87.4	87.1	66.1	148.7	44.8	44.2	50	27	148.8

a monoclinic structure at room temperature (Tab. 1) and transforms to a tetragonal and cubic phase at increasing temperature. The high temperature polymorphs can also be stabilized by the addition of suitable oxides. These partially or fully stabilized zirconia alloys have applications in fuel cells or oxygen sensors. This has motivated numerous studies on crystal structure and mechanism of transformation of zirconia polymorphs [24], electronic structure and optical properties [25]. Monoclinic ZrO_2 has 13 independent elastic constants.

2 Computational details

The DFT based ab-initio simulations were performed with the Cambridge Serial Total Energy Package (CASTEP) code [26]. A plane wave basis set is used for expanding electronic states in the pseudopotential approximation. Plane-waves are a simple way of representing electron wave functions in a periodic system. They offer a complete basis set that is independent of the type of crystal and treats all areas of space equally. This is in contrast to some other basis sets which use localized functions such as Gaussians which are dependent on the positions of the ions. Plane waves are included with energies up to a cutoff energy (Tab. 2). The norm-conserving and ultrasoft pseudopotentials [27,28] from the CASTEP database for the computations (Tab. 2) have been employed. Exchange-correlation effects were taken into account using the generalized gradient approximation (GGA) in the efficient formulation of Perdew, Burke and Ernzerhof [29,30]. Reciprocal space integration in the Brillouin zone is performed by summation over k-points with a Monkhorst-Pack grid [31]. The number of k-points necessary for converged results differs between structures due to symmetry and the degree of dispersion in electronic states (Tab. 2). With the computational parameters applied here a very high level of convergence of elastic parameters is achieved.

Two sets of computations have been carried out. The first set of calculation was performed to obtain the static equation of state (EOS) of the ceramics. Internal and external degrees of freedom were optimized for a number of structures (at constant volume), typically covering a compression range 0.8 to 1.06 relative to the experimental zero pressure volume (Tabs. 1 and 2). Computed total energies were then used to fit a finite strain equation of state [32], in order to obtain the zero pressure volume (V_0), the bulk modulus (B_0) and its pressure derivative (B_0'). In the second set of computations the elastic coefficients of the ceramics at experimental zero pressure volume have been determined. Elastic constants were computed from stress-strain relations, using positive and negative values for a specific strain (up to a strain amplitude of 0.003), and elastic constants were determined from a linear fit of the calculated stress as function of strain. For the five and six independent coefficients for the hexagonal [33] and tetragonal systems [34], two strains, one with non-zero first and fourth components, and another with non-zero third component, give stresses related to all elastic constants. For cubic systems one strain pattern is sufficient [35], whereas for ZrO_2 monoclinic four strain patterns were generated [36].

3 Results and discussions

3.1 Equation of state

DFT based computations using LDA typically overbond compounds and hence predict equilibrium volumes smaller than in experiment. GGA corrects for this and one usually obtains better agreement with experiment. An overall good agreement of the zero pressure volume computed with that in experiments was found (Tab. 3), within 4% of one another, and only the TiO_2 compounds have a zero pressure volume that is bigger than in experiment, with GGA overcorrecting the LDA shortcoming. The situation for the compression behavior and hence the bulk modulus is less satisfying (Tab. 3). While for most ceramics studied the computed bulk modulus (at computed zero pressure volume) is within 10% of ambient condition experiments the one for anatase is bigger by almost 25% and for α-SiC by 16%. These values are considerably larger than computational results previously reported in the literature which use energy-volume relations to fit an equation of state [37,38]. These studies, however, use a Hartree-Fock formalism or the LDA approximation to exchange and correlation, respectively. Due to the restricted volume range considered in the computations (Tab. 2), for all calculations a value of $B_0' = 4.0$ was determined. The consideration of a wider compression range would change this parameter.

Table 3. Equation of state parameters of the ceramic compounds. The first line of the table gives fit parameters for the computational results for the zero pressure volume (V_0), the bulk modulus at this pressure (B_0) and its pressure derivative. Calculated results (given in the first line of material) are compared with experimental equation-of-state parameters (see the second line of materials).

	V_0 [A^3]	B_0 [GPa]	B_0'
Al_2O_3	82.0	241	4.0
	84.9	254[a]	4.3[b]
α-SiC	79.6	260	4.0
	82.4	224[c]	
β-SiC	79.4	220	4.0
	82.2	220[d]	
TiO_2 rut.	63.3	235	4.0
	62.5	212[e]	6.3[f]
TiO_2 anat.	138.3	221	4.0
	135.5	179[g]	4.5[g]
CaF_2	41.6	78	4.0
	41.6	81[h]	5.2[h]
AlN	39.8	210	4.0
	40.8	211[i,j]	6.3[i,j]
BN	46.3	362	4.0
	47.2	400[k,j]	4.5[k,j]
TiB_2	25.2	251	4.0
	25.5	237[l,m]	2.0[l,m]
ZrO_2	142.4	174	4.0
	140.5	187[n]	

[a] reference [4]; [b] reference [40]; [c] reference [41]; [d] reference [42]; [e] reference [43]; [f] reference [44]; [g] reference [37]; [h] reference [45]; [i] reference [46]; [j] reference [48]; [k] reference [47]; [l] reference [49]; [m] reference [50]; [n] reference [51].

3.2 Elastic constants

Individual elastic constants (evaluated at the experimental zero pressure volume) can differ significantly between computations and experiment, but these differences are hard to quantify for all the materials studied (Tab. 4). The results obtained here are in good agreement with previous computations using GGA (where available). Instead of considering elastic constants separately, the results were quantified by computing the aggregate moduli in the Reuss-Voigt bounds [39] from the individual elastic constants (Tab. 4). The bulk and shear moduli were obtained for all considered materials (Fig. 1). In addition, the anisotropy ratios for the longitudinal (c_{22}/c_{11} and c_{33}/c_{11}) and shear elastic constants (c_{55}/c_{44} and c_{66}/c_{44}) (Fig. 2) have been computed. These ratios are a measure of the relative propagation of the longitudinal and transverse acoustic velocities along the three crystallographic axes, respectively.

For the bulk modulus derived from the elastic constant tensor (Fig. 1a, Tab. 4), a much better agreement (within 5%) with experiment than for that from the equation of state could be found. This better agreement justifies and suggests the use of the experimental zero pressure volume to evaluate elastic parameters of materials rather than the computational equilibrium volume. Similar to the

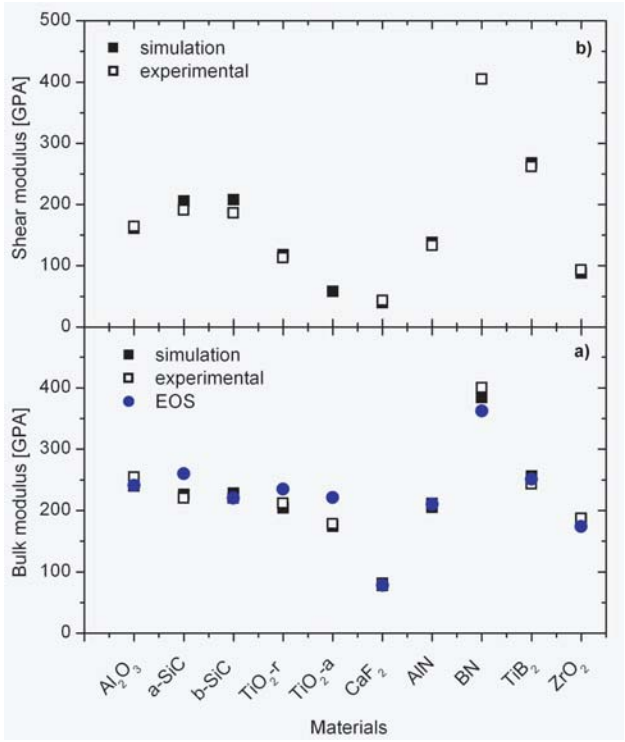

Fig. 1. Comparison between experimental (□ experimental) and simulated (■ simulation) bulk and shear modulus for the studied ceramics. For the computational bulk modulus both the one obtained from the equation-of-state (● EOS) and the one obtained from averaging the single crystal elastic constants are given.

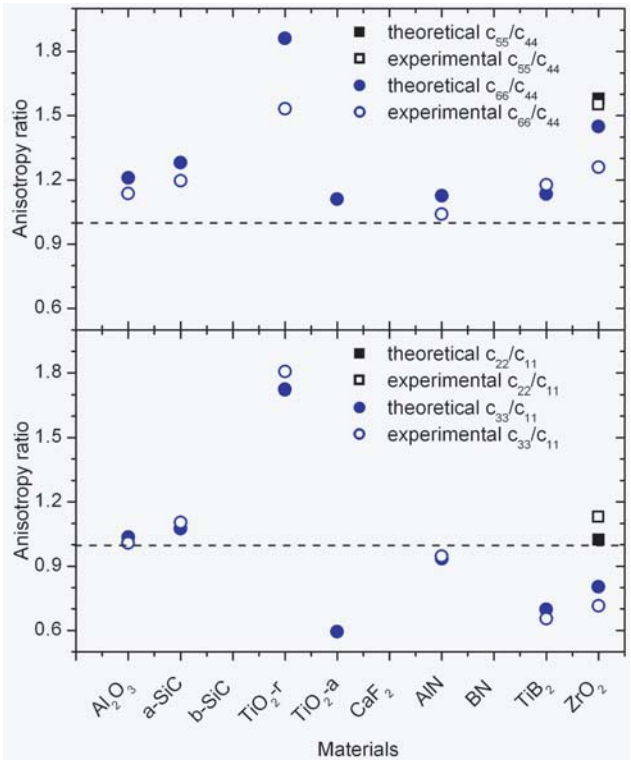

Fig. 2. Anisotropy ratios for the longitudinal (bottom) and shear elastic moduli (top) for experiments and computations.

Table 4. Elastic constants of the studied ceramic materials (in GPa). The first line of the table gives the elastic constants c_{ij} for each material, presented in the first column. The first line of each material presents the calculated data and the second one the experimental values (italic characters), which were taken from references mentioned below. The last two columns show the theoretical and experimental bulk and shear modulus which are the arithmetic average of Reuss and Voigt [39] values, calculated using the theoretical and experimental c_{ij}, respectively.

Mat.	Method	C_{11}	C_{22}	C_{33}	C_{44}	C_{55}	C_{66}	C_{12}	C_{13}	C_{15}	C_{23}	C_{25}	C_{35}	C_{46}	B	G
Al_2O_3 rhom	**This work**	**484**		**501**	**138**		**167**	**150**	**99**	**27**					**240**	**161**
	PP-PW[a]	495		486	148		162	171	130	20					259	160
	Experiments[b]	497		501	147		167	163	116	22					254	164
α-SiC hexag	**This work**	**534**		**574**	**171**		**219**	**96**	**50**						**226**	**206**
	Experiments[c]	501		553	163		195	111	52						220	191
β-SiC cubic	**This work**	**420**			**267**			**132**							**228**	**208**
	FP-LMTO-LDA[d]	420			287			126							224	220
	Experiments[e]	379			252			141							220	186
TiO_2-r tetrag	**This work**	**278**		**479**	**115**		**214**	**153**	**149**						**204**	**118**
	Experiments[f]	268		484	124		190	175	147						212	113
TiO_2-a tetrag	**This work**	**320**		**190**	**54**		**60**	**151**	**143**						**174**	**58**
	Experiments[g]	- - -		- - -	- - -		- - -	- - -	- - -						178	- - -
CaF_2 cubic	**This work**	**155**			**31**			**39**							**78**	**40**
	FP-LAPW-GGA[h]	146			43			50							77	51
	PP-LCAO-GGA[i]	159			35			40							76	48
	PP-PW-LDA[j]	183			34			61							83	66
	Experiments[k]	165			34			39							81	43
AlNhexag	**This work**	**413**		**386**	**126**		**142**	**129**	**96**						**205**	**138**
	PP–LDA[l]	398		383	127		128	142	112						212	130
	FP-LMTO-LDA[m]	398		382	96		129	140	127						218	116
	PP-PW-LDA[n]	380		382	109		133	114	127						208	121
	PP-PW-LDA[o]	396		373	116		130	137	108						207	126
	Experiments[p]	411		389	125		130	149	99						211	133
BN cubic	**This work**	**816**			**469**			**168**							**384**	**405**
	FP-APW+lo-	834			495			189							404	417
	LDA[q]	837			493			182							400	418
	FP-LMTO-LDA[m]	819			475			195							403	401
	PP– LDA[l]	812			464			182							392	397
	PP-PW-LDA[r]															
	Experiments[s]	820			480			190							400	405
TiB_2 hexag	**This work**	**671**		**468**	**269**		**305**	**62**	**103**						**256**	**268**
	Experiments[t]	660		432	260		306	48	93						243	262
	PP-PW-GGA[u]	656		461	259		295	66	98						240	265
	PP-PW-LDA[u]	709		506	295		319	71	117						280	287
ZrO_2 mono	**This work**	**341**	**349**	**274**	**80**	**73**	**116**	**158**	**88**	**29**	**156**	**−4**	**2**	**−14**	**187**	**88**
	Experiments[v]	361	408	258	100	81	126	142	55	−21	196	31	−18	−23	187	93

[a] reference [5]; [b] reference [4]; [c] reference [41]; [d] reference [55]; [e] reference [42]; [f] reference [43]; [g] reference [47]; [h] reference [52]; [i] reference [53]; [j] reference [54]; [k] reference [15]; [l] reference [56]; [m] reference [48]; [n] reference [60]; [o] reference [61]; [p] reference [46]; [q] reference [56]; [r] reference [58]; [s] reference [47]; [t] reference [49]; [u] reference [59]; [v] reference [51]. FP = Full Potential; PP = Pseudopotential; PW = Plane-Wave; LAPW = Linear Augmented Plane-Wave; LMTO = Linear Muffin Tin Orbitals; LCAO = Linear Combination of Atomic Orbitals; APW+lo = Augmented-Plane Wave plus Local Orbitals.

bulk moduli, the shear moduli determined from the computations are in overall good agreement with experiment, with a maximum deviation of 10% (or 20 GPa) for the SiC polytypes (Fig. 1b, Tab. 4). Typically it was found that the shear moduli of the stiffer materials are overpredicted, while those of the softer materials are underpredicted.

The comparison of anisotropy ratios between experiments and computations provide a similarly good picture (Fig. 2). Regardless of the system and anisotropy type, the correct sense of anisotropy (fast vs. slow propagation direction of acoustic waves) was predicted. The materials that show strongest anisotropy in experiment, TiO_2 rutile and ZrO_2 for shear anisotropy and TiO_2 rutile and TiB_2 for longitudinal anisotropy, are predicted with the strongest anisotropy in the computations.

Comparing our results and previous computations with experiments we find again that GGA provides an overall better description of elastic constants of the ceramic materials studied here.

4 Conclusions

DFT based ab-initio calculations of elastic properties for a number of ceramic materials: Al_2O_3, SiC, TiO_2, AlN, BN, TiB_2, CaF_2, ZrO_2 have been carried out. The full elastic constant tensor at the experimental zero pressure volume was computed. It can be concluded that ab-initio methods with the GGA approximation are capable of reproducing the most important features in elastic behaviour: the aggregate moduli as well as the general sense of anisotropy in longitudinal and shear moduli. These results show that modern ab-initio computations can be used independently from experiment to predict elastic stability, and can provide a basis for the modelling of structural and elastic properties of more complex aggregate ceramic materials.

The authors thank the Fraunhofer Gesellschaft for financial support within the joint project "MAVO-Multiscale Modelling", and partial support through the Elitenetzwerk Bavaria.

References

1. D.W. Richerson, *Modern Ceramic Engineering: Properties, Processing, and Use in Design*, 2nd edn. (Marcel Dekker, Inc., New York, 1992)
2. H.J. McSkimin, J. Acoustical Soc. Am. **33**, 12 (1961)
3. M.J. Damzen, *Stimulated Brillouin Scattering, Fundamentals and Application* (Institute of Physics, Bristol, 2003)
4. T. Goto, O.L. Anderson, I. Ohno, S. Yamamoto, J. Geophys. Res. **94**, 7588 (1989)
5. J.R. Gladden, J.H. So, J. Maynard, P.W. Saxe, Y.L. Page, Appl. Phys. Lett. **85**, 392 (2004)
6. J. Boettger, Phys. Rev. B **55**, 750 (1997)
7. S.-D. Mo, W.Y. Ching, Phys. Rev. B **57**, 15219 (1995)
8. A.R. Verma, P. Krishna, *Polymorphism and Ploytypism in Crystals* (Wiley, New York, 1966)
9. Y.-M. Chiang, D. Birnie III, W.D. Kingery, *Physical Ceramic* (Wiley, New York, 1997)
10. K.M. Glassford, J.R. Chelikovsky, Phys. Rev. B **46**, 1284 (1992)
11. S.-D. Mo, W.Y. Ching, Phys. Rev. B **51**, 13023 (1995)
12. V. Milman, *Properties of Complex Inorganic Solids*, edited by A. Gonis, A. Meike, P.E.A. Turchi (Plenum Press, New York, 1997)
13. J. Muscat, V. Swamy, N.M. Harrison, Phys. Rev. B **65**, 224112 (2002)
14. E. Stoyanov, F. Langenhorst, G. Steinle-Neumann, American Mineralogist **92**, 577 (2007)
15. C.R.A. Catlow, J.D. Comins, F.A. Germano, R. Tharley, W. Hayes, J. Phys. C **11**, 3197 (1978)
16. P.S. Ho, A.L. Ruoff, Phys. Rev. **161**, 864 (1967)
17. D. Gerlich, Phys. Rev. **135**, A1331 (1964); D. Gerlich, Phys. Rev. **136**, A1366 (1964)
18. M. Catti, R. Dovesi, A. Pavese, V.R. Saunders, J. Phys.: Condens. Matter **3**, 4151 (1991)
19. J.J. Pouch, S.A. Alterowitz, *Synthesis and Properties of Boron Nitride,* Material Science Forum (Aldersmannsdorf, Trans Tech, 1990), Vol. 54
20. G. Mueller, F. Raether, L. Jacobsen, in *9th Cimtec-World Ceramics Congress, Ceramics: Getting into the 2000's – Part B*, edited by P. Vincenzini (Techna Srl, 1999)
21. F. Raether, A. Klimera, A. Thimm, J. Ruska, B. Mussler, D. Brunner, Materials Week, Symp. K5 Multifunctional Ceramics (Munich, Germany, 2001)
22. R.G. Munro, J. Res. Natl. Inst. Stand. Technol. **105**, 709 (2000)
23. I.V. Matkowich, *Boron and Refractive Borides* (Springer, New York, 1977)
24. G. Jomard, T. Petit, A. Pasturel, L. Magaud, G. Kresse, J. Hafner, Phys. Rev. B **59**, 4044 (1999)
25. R.H. French, S.J. Glass, F.S. Ohuchi, Y.-N. Xu, W.Y. Ching, Phys. Rev. B **49**, 5133 (1994)
26. M.D. Segall, P.L.D. Lindan, M.J. Probert, C.J. Pickard, P.J. Hasnip, S.J. Clark, M.C. Payne, J. Phys.: Condens. Matter **14**, 2717 (2002)
27. D. Vanderbilt, Phys. Rev. B **41**, 7892(1990)
28. J.S. Lin, A. Qteish, M.C. Payne, V. Heine, Phys. Rev. B **47**, 4174 (1993)
29. J.P. Perdew, Y. Wang, Phys. Rev. B **45**, 1324 (1992)
30. J.P. Perdew, K. Burke, M. Ernzerhof, Phys. Rev. Lett. **77**, 3865 (1996)
31. H.J. Monkhorst, J.D. Pack, Phys. Rev. B **13**, 5188 (1976)
32. F. Birch, J. Geophys. Res. **57**, 227 (1952)
33. V. Milman, M.C. Warren, J. Phys.: Condens. Matter **13**, 241 (2001)
34. J. Lazewski, K. Parlinski, J. Chem. Phys. **114**, 6734 (2001)
35. R.B. Karki, J.L. Stixrude, S.J. Clark, M.C. Warren, G.J. Ackland, J. Crain, American Mineralogist **82**, 51 (1997)
36. N.T.S. Lee, V.B.C. Tan, K.M. Lim, Appl. Phys. Lett. **88**, 031913 (2006)
37. T. Arlt, M. Bermejo, M.A. Blanco, L. Gerward, J.Z. Jiang, J. Staun Olsen, J.M. Recio, Phys. Rev. B **61**, 14414 (2000)
38. P. Kaeckell, B. Wenzien, F. Bechstedt, Phys. Rev. B **50**, 17037 (1994)
39. A. Reuss, Z. Angew. Math. Mech. **9**, 49 (1929); W. Voigt, Wied. Ann. **38**, 573 (1889)
40. H. d'Amour, D. Schiferl, W. Denner, H. Schulz, W.B. Holzapfel, J. Appl. Phys. **49**, 4411 (1978)
41. K. Kamitani, M. Grimsditch, J.C. Nipko, C.K. Loong, M. Okada, I. Kimura, J. Appl. Phys. **82**, 3152 (1997)
42. R.F.S. Hearmon, *Numerical data and functional relationships in science and technology* (Landolt Bornstein, Springer-Verlag, 1984), Band 11/Vol. 11
43. D.G. Isaak, J.D. Carnes, O.L. Anderson, H. Cynn, E. Hake, Phys. Chem. Minerals **26**, 31 (1998)
44. M.H. Manghnami, J. Geophys. Res. **74**, 4317 (1969)
45. R.J. Angel, J. Phys.: Condens. Matter **5**, L141 (1993)
46. L.E. McNeil, M. Grimsditch, R.H. French, J. Am. Ceram. Soc. **76**, 1132 (1993)
47. M. Grimsditch, E.S. Zouboulis, A. Polian, J. Appl. Phys. **76**, 832 (1994)
48. K. Kim, W.R. Lambrecht, B. Segall, Phys. Rev. B **53**, 16310 (1996)
49. P.S. Spoor, J.D. Maynard, M.J. Pan, D.J. Green, J.R. Hellmann, T. Tanaka, Appl. Phys. Lett. **70**, 1959 (1997)
50. D.P. Dankedar, D.C. Benfanti, J. Appl. Phys. **73**, 673 (1993)
51. S.-C. Chan, Y. Fang, M. Grimsditch, Z. Li, M. Nevitt, W. Robertson, E.S. Zoubolis, J. Am. Ceram. Soc. **74**, 1742 (1991)

52. R. Khenata, B. Daoudi, M. Sahnoun, H. Baltache, M. Rerat, A.H. Reshak, B. Bouhafs, H. Abid, M. Driz, Eur. Phys. J. B **47**, 63 (2005)
53. M. Merawa, M. Llunell, R. Orlando, M.G. Duvignau, R. Dovesi, Chem. Phys. Lett. **368**, 7 (2003)
54. Z.H. Levine, J.H. Burnett, E.L. Shirley, Phys. Rev. B **68**, 155120 (2003)
55. W.R.L. Lambrecht, B. Segall, M. Methfessel, M. van Shilfgaarde, Phys. Rev. B **44**, 3685 (1998)
56. M.B. Kanoun, A.E. Merad, G. Merad, J. Cibert, H. Aourag, Solid-State Electronics **48**, 1601 (2004)
57. K. Shimada, T. Sota, K. Suzuki, J. Appl. Phys. **84**, 4951 (1998)
58. K. Karch, J.M. Wagner, F. Bechstedt, Phys. Rev. B **57**, 7043 (1998)
59. V. Milman, M.C. Warren, J. Phys.: Condens. Matter **13**, 5585 (2001)
60. R. Kato, J. Hama, J. Phys.: Condens. Matter **6**, 7617 (1994)
61. A.F. Wright, J. Appl. Phys. **82**, 2833 (1997)